Rochester Institute of Technology

RIT Digital Institutional Repository

8-8-1993

Advanced Lithography Simulation Tools for Development and Analysis of Wide-Field High Numerical Aperture Projection Optical Systems

James E. Connors
GCA/Tropel

Todd Kos
GCA/Tropel

Robert C. Pack
R.C. Pack Associates

Bruce W. Smith
Rochester Institute of Technology

Follow this and additional works at: https://repository.rit.edu/other

Recommended Citation

Advanced lithography simulation tools for development and analysis of wide-field high NA projection optical systems

James E. Connors, Todd M. Kos, Robert C. Pack*, Bruce W. Smith**

GCA Tropel, a Unit of General Signal
Fairport, NY

*R.C. Pack and Associates
Portola Valley, CA

**Rochester Institute of Technology
Rochester, NY

ABSTRACT

Industrial demands for integrated circuits of higher speed and complexity have required the development of advanced lithographic exposure tools capable of sub-half micron resolution over increasingly larger fields. To this end, i-line and deep-uv tools employing variable, high numerical aperture (NA) objectives are being aggressively developed. The design and manufacture of these advanced optical systems has also grown in complexity, since tighter tolerances on resolution and image placement must be maintained over the larger lens field. At the same time, usable focus and exposure latitude must be retained. The influence of lens aberrations on image formation under different illumination conditions, along with their non-intuitive nature has required the development of simulation tools that allow both the designer and the user of these systems to better understand their implications. These tools can be used to investigate and optimize the lithography process, including the effects of emerging technologies such as phase-shift masking, oblique illumination and frequency plane filtering.[1,2,3] This paper presents a method for determining the effects and interactions of various aberrations and illumination conditions using a statistically designed experiment.[4] Fundamental differences in the way the aerial image is formed when varying the pupil energy distribution in the presence of aberrations are presented, as are examples of some of the more interesting effects.

1. INTRODUCTION

As device dimensions shrink below 0.5 μm, the need arises for simulation tools that are capable of handling some of the unique challenges presented by variable, high numerical aperture objectives and larger field sizes. One effect of using these objectives is additional higher frequency aberrations which impact image formation.[5] Residual aberrations of a wide-field high-NA lens are difficult to minimize during both design and fabrication,[6] and their effect on image formation is not intuitive. Additionally, the influence of these aberrations throughout the field may change as the aperture size and illumination are optimized for each chip layer. Lithography simulation software is available that can assist the designer and user of these systems better to understand and optimize the process window. Because of the complexity and growing number of variables that impact lithographic performance, statistical and experimental methods are effective in collecting and analyzing simulation results. For this experiment, a commercially available simulator is used that allows the wave aberration function of the imaging objective to be described using the orthogonal Fringe Zernike polynomials.[7,8] In addition, the intensity distribution in the pupil can be defined functionally to study the effects of non-uniform, de-centered

and off-axis illumination. The objective wavefront can originate from the lens design software, or from a phase-measured interferogram (PMI) of an assembled lens system.[9] Wavefronts from numerous field points can be investigated simultaneously to optimize full-field lens performance.

With the increasing interest in exposure tools that employ variable numerical aperture,[10] coherence and off-axis illumination, there are 2 fundamental issues to consider: First, varying illumination changes the weighting of the pupil function, and second, varying linewidth or type of feature changes the sampling of the lens pupil. These are significant issues when dealing with optical systems that are aberration-limited. Figure 1a shows an example of a wavefront generated using lens aberration data. The magnitude of the optical path difference (OPD) in this figure is representative of what is tolerable in a lens designed for 0.25 μm resolution. Figure 1b shows the energy distribution in the lens pupil for 0.25 μm dense lines oriented along the x-axis. At NA=0.53, σ=0.75 and λ=248 nm, only the zero and ± 1 diffracted orders fall inside the aperture. Figure 1c shows the effective pupil function, or the part of the wavefront that acts to degrade the image. In this case, parts of the pupil near the edge are not used, and aberrations at those locations do not influence image formation for this particular feature.

This type of lithography simulation has been used successfully in understanding the CD variation of wide-field lenses. For example, Figures 2a and 2b show the aerial image width versus defocus plots for 0.35 μm features using a 0.53 NA objective, and a condenser NA of 0.265 (σ=0.50) and 0.398 (σ=0.75) respectively. Each plot contains 10 points from axis to the edge of the field, and 2 feature orientations (sagittal and tangential). The difference in field dependence and flatness of the curves can be attributed to the amount of interference between the -1, 0 and +1 diffracted orders.[3] More 2-beam (±1 order) and less 3-beam (-1, 0 and +1 orders) interference effectively makes the image less sensitive to defocus, and therefore the variation in the width of the image through focus is minimized.

The effects of annular illumination appear in Figures 3a and b. Notice that a large portion of the wavefront is not used in this case. As Figure 4 demonstrates, the energy distribution changes with the object as well, in this case 0.25 μm lines on an alternating phase mask using annular illumination. Clearly, the illumination would need to be re-positioned for the frequency-doubled object, which would use yet another part of the pupil. Because of this growing complexity, determination of the sensitivities of all factors contributing the formation of the image requires statistical methods. As an example, an experiment has been designed to evaluate the influence of lens aberrations under various illumination conditions. Behavior of the aerial image was investigated for uniform, annular and quadrupole illumination with an aberrated pupil. This methodology can easily be applied to lithography simulation in general.

2. SIMULATION

2.1 Aerial image calculation

Projected aerial images are calculated by the simulator using the well-known Hopkins approach.[11] In this case, the wave aberration function is expanded as a sum of radial Zernike polynomials, which are convenient for circular apertures. The wavefront (phase error) in the objective pupil can be generated using lens design software, or phase-measured interferograms (PMI). The simulator accepts the pupil function in terms of coefficients which are then multiplied by their respective polynomials. Each Fringe Zernike term (Table 1) describes uniquely the deviations between the spherical wavefront emanating from an ideal lens and the actual wavefront. In each Zernike term, defined over the unit aperture, R is the radial position and α is the phase angle. Chromatic aberrations can also be simulated if the behavior of the wavefront is known over the bandwidth of the source. The illuminator intensity distribution can be specified in a grid or functional form for easy comparison of various illumination schemes.

2.2 Aerial image metrics

One important challenge when analyzing an aberration-limited optical system is choosing metric or metrics for judging aerial image quality. Although conventional metrics like image contrast and slope[12] are becoming more useful as higher contrast photoresists become available, they do not convey any information about the bulk of the image. The strehl and line ratios relate the quality of the image to the diffraction-limited case, but only by peak intensity. For this experiment, we have used a measure that attempts to compare the aberrated image to the diffraction-limited case by looking at the difference in area under the curve. The Total Image Deviation (TID) is calculated by first estimating and removing the image placement error (IPE) such that the 30% relative intensity threshold is centered about the nominal mask (see Fig. 5). Then equation 1 is applied, which sums the absolute value of the differences in relative intensity over 1 mask period.

$$TID = \sum_{x=0}^{2*CD} |I_{perfect} - I_{aberrated}| \tag{1}$$

Because the TID measures a deviation from nominal, a number closer to zero corresponds to a better image. This metric works equally well for dense and isolated features, and can be expanded to 2-dimensions for contact holes and islands. It also allows for easy comparison of illumination conditions where the nominal image is changing from one case to the next. The symmetry of the image is also an important characteristic. An estimate of the image symmetry can be made by evaluating the difference in slope on either side at some reference intensity level, in this case 30% (Figure 5).

2.3 Positioning of illumination

Positioning of the intensity distribution in the pupil was accomplished by using equation 2 to optimize the performance of 0.25 µm dense lines.[3]

$$\theta_i = \sin^{-1}(\lambda/2p) \tag{2}$$

Where θ_i is the optimum incident illumination angle, λ is the illumination wavelength, and p is the period of the mask feature to be imaged. The uniform illumination ($\sigma=0.765$) was centered in the pupil, and the annular obscuration blocked 73.8% of the area. The quad poles were centered at 0.665σ and have a radius of 0.10σ. The relative area of the off-axis intensity distribution was chosen based on realistic throughput requirements.

3. EXPERIMENTAL DESIGN

The object being imaged by the lithography simulator is a transmission mask containing dense 0.25 µm lines and spaces in the radial (saggital) orientation. The operational parameters of the exposure system are NA=0.53 and λ=248.4 nm, using the three illumination schemes discussed in section 2.3. The factors for this experiment were 29 of the 37 orthogonal Fringe Zernike terms, and defocus. Piston, power and x and y tilt terms (Z1-Z4) were omitted, as were 90° phase terms because they do not affect the sagittal orientation (marked with # in Table 1). There are several advantages to using a designed experiment (DOE) over the Monte Carlo or 1 factor-at-a-time methods of simulation.[13] The designed experiment approach was chosen because it offers benefits of evaluating many factors simultaneously, identification of interactions, and easier interpretation of results through Analysis of Variance (ANOVA). Additionally, a designed experiment can more accurately measure variability, and more precisely estimate factor effects.

3.1 Experimental design matrix and parameters

In order to sufficiently determine the effects of 30 variables, a design that studies the factors at three levels (low, nominal and high) was chosen. One way to evaluate these factors is by using a full-factorial design which investigates all possible treatment combinations. This would require 3^{30} runs, which would demand an enormous amount of computer time. As an alternative, a $3_{III}^{(7-3)}$ fractional factorial, or Taguchi's L81 design matrix[14] was utilized in two phases. The first phase involved performing a series of screening experiments to identify important aberrations and interactions. The results from the screening tests were compiled, and a special L81 design matrix was constructed for the second phase of experimentation. All L81 experiments had aberration factors set to -0.05, 0 and +0.05 waves, and focus varied by ±0.1 μm around the nominal setting of zero. These levels were chosen such that they would degrade, but not completely destroy the image. The simulation yielded responses for Total Image Deviation (TID), image symmetry, and image placement error as defined in section 2.2.

3.2 Screening experiments and final design

The orthogonal nature of the Fringe Zernikes permitted the rapid identification of important effects using five-factor screening experiments. These 3-level experiments (interactions studied shown in Fig. 7a) included looking at various combinations of up to 9th order astigmatism and coma, up to 11th order spherical aberration, and defocus. Shown in Figure 7b are the linear graphs[14] for the 11 most influential factors and interactions, selected as a result of the screening experiments. Using the Taguchi interaction table, these factors were carefully assigned to the columns of the L81 matrix. The numbers represent the terms of the Fringe Zernike polynomials (also marked with * in Table 1). It is important to note that the factors deemed significant are by no means the only aberrations the lithography engineer need be concerned with. The validity of the results is bounded by the experimental space, and one could easily reach a different conclusion if another size or type of feature were to be studied.

4. RESULTS AND ANALYSIS

The overall results of the experiment appear in Table 2, namely the relative influence each factor has on the responses under the 3 illumination conditions. Unshaded areas in Table 2 indicate statistically significant contributions to the given response. Notice the varying degree of influence from one illumination scheme to the next. In some cases, such as 3rd order astigmatism and focus, the contribution changes from very significant to relatively insignificant. Also, some factors that were significant in the screening experiments, contributed little to the variation when studied in the final design. Because the symmetry of the image is nearly perfect for the annular and quadrupole cases (see the MIN and MAX values at the bottom of the table), the analysis of variance rendered many of the sensitivities for this response statistically insignificant. In the uniform case however, the ratio of symmetry variation to the noise is extremely high, thus identifying significant factors of interest.

4.1 Aerial image examples

In Figures 8-14 are examples of the more influential factors highlighted in Table 2. Aerial images are shown for uniform and quadrupole illumination only, as they differ most drastically. Also, the magnitude of the aberrations in these examples has been increased beyond the experimental factor levels for viewing purposes. Figures 8a and b show the differing effect of 3rd order coma (Z7) under uniform and quad illumination. Similar comparisons follow in Figures 9-11 for 3-point (Z10), 5th order coma (Z14) and 5th order 3-point (Z19). The comatic terms have a much greater effect on symmetry under conventional illumination than the off-axis cases, but this is a function of the width of the annular ring, the area of the poles and the linewidth. A combination of defocus and 3rd order astigmatism (Z5) is shown in Figure 12, where the quad illumination appears to be less sensitive to this interaction, consistent with recent works explaining this phenomenon.

In Figure 13, the interaction between 3rd and 5th order 45° astigmatism (Z6 and Z13) appears much stronger for the quad illumination. Similar to focus and astigmatism, Figure 14 shows that third order spherical aberration (Z9) is more influential under uniform illumination.

4.2 Experiment responses

In order to study the entire experimental space, it is convenient to construct response surfaces of highly significant factors. The TID response surface for 3rd and 5th order 45° astigmatism (Fig. 15) clearly shows the strong interaction between these terms as well as the difference between uniform and quad illumination. Similarly, Figure 16 shows the difference in sensitivity of phase-shift (IPE) to 3rd order coma and 5th order 3-point, and the lack of an interaction term. Histograms provide additional insight of the three responses: Figure 17 shows the increasing magnitude of IPE when going from uniform to annular to quad illumination. Figure 18 shows the frequency distribution of the TID statistic, where the strong interaction between Z6 and Z13 shows up very clearly in the quad case. Figure 19 shows image symmetry variation to be much less for both off-axis types of illumination.

4.3 Analysis

The underlying reason for these differences is the changing energy distribution (weighting) in the pupil, as discussed in section 1. Consider for example the 1-dimensional case of pure 3rd order comatic aberration. Figure 20 shows the coma as the deviation from a spherical wavefront. In this example the illumination is positioned such that the diffracted orders use part of the wavefront which "looks" like pure tilt (or distortion), and since the center of the wavefront is not used, the resulting aerial image formed is shifted in phase, but very symmetrical. This image placement error is not distortion in the conventional sense, because it is linewidth dependent. In other words, the phase-shift could be removed by simply tilting the wavefront, but this compensation would only apply for a given linewidth. To show how this might effect full-field lens performance, Figure 21 is an example of how radial image placement error would change for 0.25 μm features under the 3 illumination conditions. The wavefront OPD at each field position is less that 0.20λ TIR, representative of what is required for 0.25 μm imaging. Figures 22a and b compare the linewidth dependence of image placement error for uniform and quadrupole illumination.

5. CONCLUSIONS

Rigorous analysis of wide-field, high NA lithographic lenses requires that the higher frequency aberrations and their field dependence be accounted for. Optimization of numerical aperture, illumination, and the other lithography "extenders" is a complex, multi-variable operation that requires a systematic engineering approach. Lithography simulators, when combined with statistical design of experiments techniques, can be used to investigate these complex imaging scenarios.[15,16] This combination yields a high ratio of information to cost (computer simulation time). This experiment enabled an investigation of several significant aberrations and interactions as the pupil energy distribution was changed from conventional to oblique. The Total Image Deviation has been suggested as a new metric that includes the bulk of the aerial image and compares it to the diffraction limited case. Significant differences in the influence of lens aberrations under varying illumination conditions were detected. The effects of the factors in this study would have been difficult to isolate without using statistical methods. Tools like these can be successfully employed to investigate and optimize various illumination, mask, and lens conditions.

6. ACKNOWLEDGMENTS

7. REFERENCES

1. D. L . Fehrs, H. B. Lovering, R. T. Scruton, "Illuminator Modification of an Optical Aligner," Proc. KTI Microlithography Seminar, pp. 217-230, Nov. 1989.

2. H. Fukuda, T. Terasawa, S. Okazaki, "Spatial Filtering for Depth of Focus and Resolution Enhancement in Optical Lithography," Proc. 35th EIPB, May. 1991.

3. W. N. Partlo, P. J. Tompkins, P. G. Dewa, P. F. Michaloski, "Depth of Focus and Resolution Enhancement for I-Line and Deep-uv Lithography Using Annular Illumination," Proc. SPIE Optical/Laser Microlithography VI, to be presented at this conference, Mar. 1993.

4. D. C. Montgomery, Design and Analysis of Experiments, pp. 414-432, John Wiley & Sons, New York, 1991.

5. J. E. Gortych, D. Williamson, "Effects of Higher-Order Aberrations on the Process Window," Proc. SPIE Laser/Optical Lithography IV, Mar. 1991.

6. A. V. Hill, J. E. Webb, A. R. Phillips, J. E. Connors, "Design and Analysis of a High NA Projection Optical System for 0.35 μm Deep-uv Lithography," Proc. SPIE Optical/Laser Microlithography VI, to be presented at this conference, Mar. 1993.

7. M. Born, E. Wolf, Principals of Optics, Pergamon Press, New York, 1980.

8. D. Malacara, J. M. Carpio-Valdez, J. J. Sanchez-Mondragon, "Wavefront Fitting with Discrete Orthogonal Polynomials in a Unit Radius Circle," Opt. Eng, vol. 29, no. 6, pp. 672-675, Jun. 1990.

9. J. E. Webb, "Measurements of Optical Performance of Photolithographic Lenses," Integrated Circuit Metrology II, Proc. SPIE vol. 480, pp. 133-140, Mar. 1984.

10. S. G. Olson, C. Sparkes, J. E. Connors, W. N. Partlo, "Optimizing NA and Sigma for Sub-Half Micron Lithography," Proc. SPIE Optical/Laser Microlithography VI, to be presented at this conference, Mar. 1993.

11. H. H. Hopkins, "On the Diffraction Theory of Optical Images," Proc. Roy. Soc, A 217, pp. 408-431, 1953.

12. C. A. Mack, "Understanding Focus Effects in Submicrometer Optical Lithography," Opt. Eng, vol. 27, no. 12, pp. 1093-1100, Dec. 1988.

13. T. B. Barker, Engineering Quality by Design: Interpreting the Taguchi Approach, ASQC Quality Press, New York, 1990.

14. G. Taguchi, "Table of Orthogonal Arrays and Linear Graphs," Reports of Stat. App. Res, Union of Japanese Scientists and Engineers, vol. 6, no. 5, pp. 1-52, 1960.

15. R. C. Pack, M. R. Kump, D. A. Bernard, W. B. Graboski, T. L. Crandle, "Optimization of the Photolithographic Process Through Coupled Process and Device Simulation and Design Centering," Proc. KTI Microlithography Seminar, pp. 257-270, Nov. 1990.

16. B. W. Smith, Wai-Man Shiao, R. Holscher, P. Mahoney, "Response Surface Modeling Utilizing Lithographic Process Simulation," Integrated Circuit Metrology VI, Proc SPIE vol. 1673, pp. 486-497, Mar. 1992.
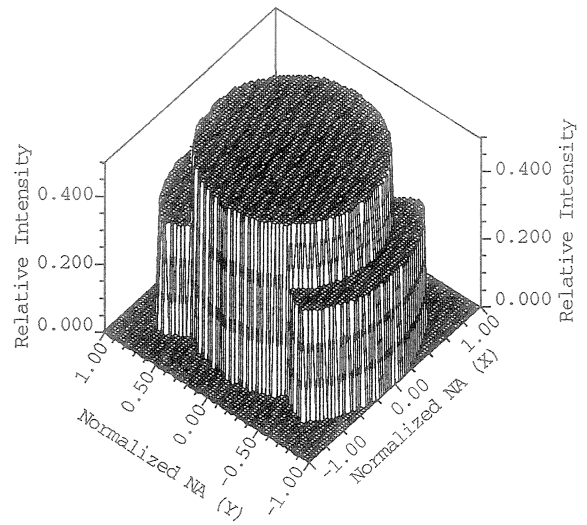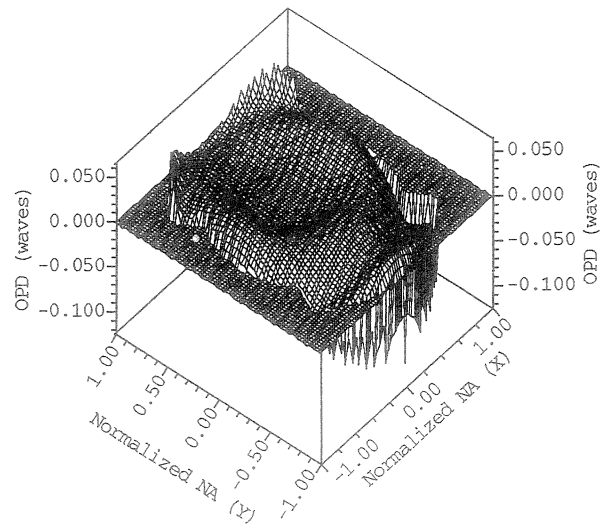
Objective Wavefront
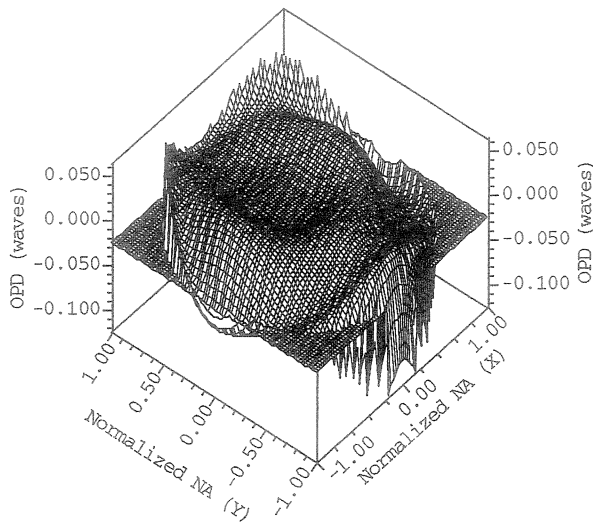
Pupil Energy Distribution

Fig 1a.

Fig 1b.

Fig 1a: Full Aperture Wavefront
NA = 0.53; Wavelength = 248 nm

Fig 1b: Conventional Illumination; 0.25 um
Dense Lines; NA = 0.53;
SIGMA = 0.74; Wavelength = 248 nm

Fig 1c: Effective Pupil Function
for 0.25 um lines from (a) and (b)

Masked Effective Pupil

Fig 1c.

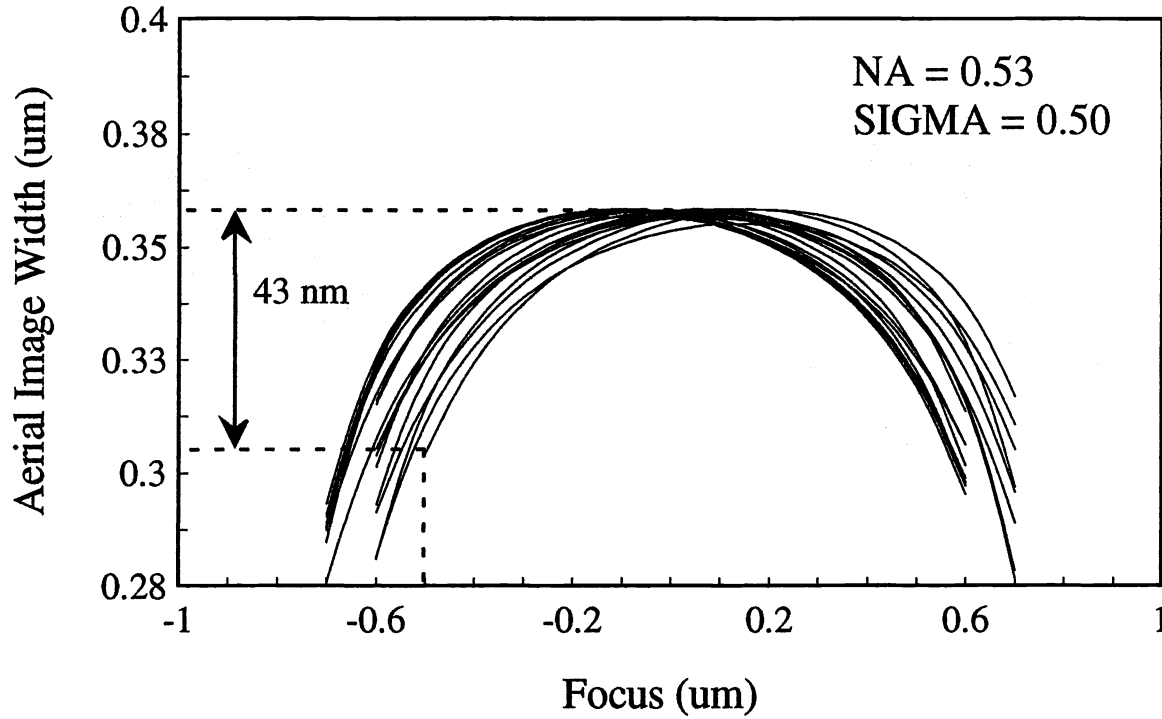# Wide-Field Aberration Analysis:
Image Width Variation with Focus

Fig. 2a
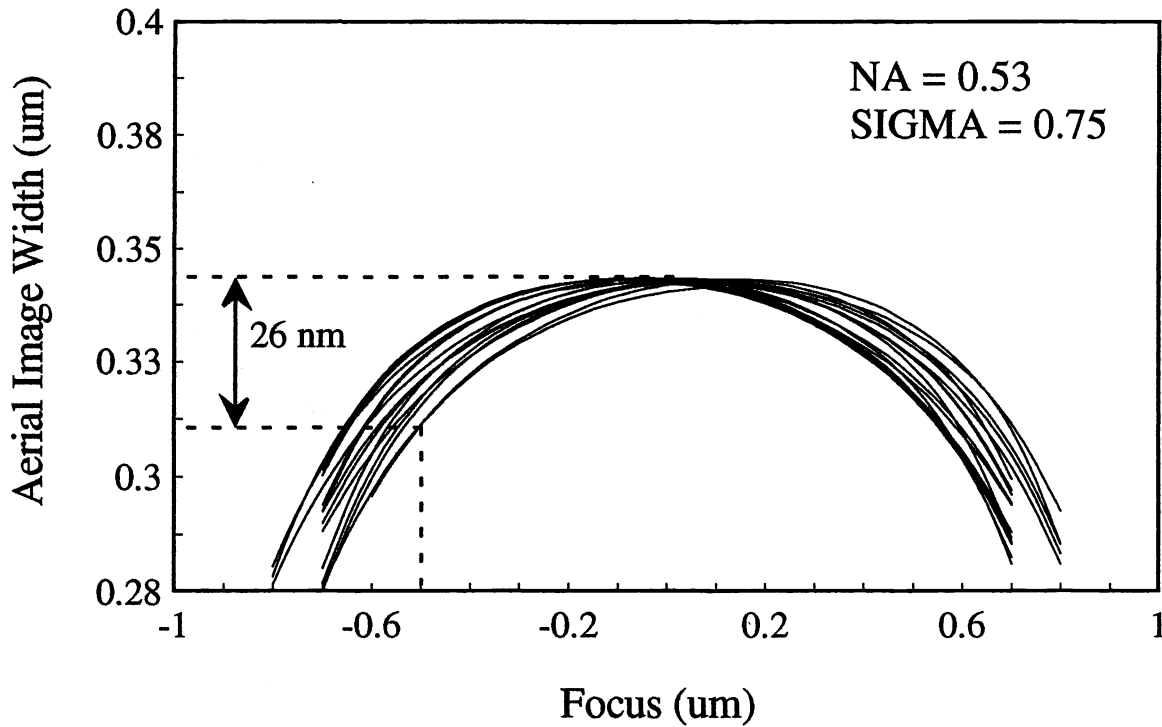
Fig. 2b
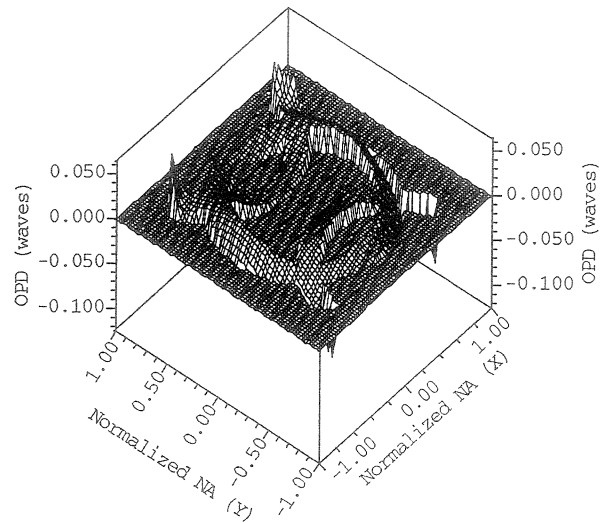
Pupil Energy Distribution
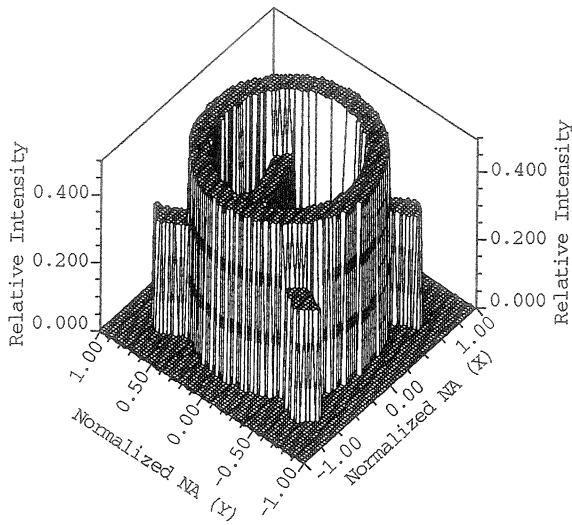
Fig 3a.

Masked Effective Pupil

Fig 3b.
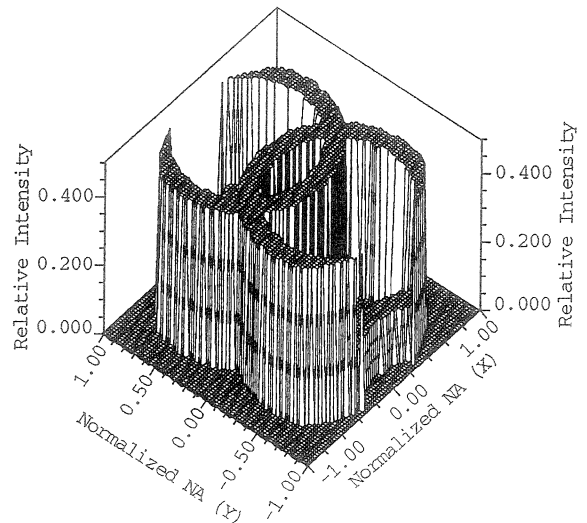
Fig 3a: Annular Illumination; 0.25 um
Dense Lines; NA = 0.53;
SIGMA = 0.74; Wavelength = 248 nm
Conventional Transmission Mask

Fig 3b: Effective Pupil Function
for 0.25 um lines from (1a) and (3a)

Fig 4: Annular Illumination; 0.25 um
Dense Lines; NA = 0.53;
SIGMA = 0.74; Wavelength = 248 nm;
Alternating Phase Mask

Pupil Energy Distribution

Fig 4.

| Term	Fringe Zernike Polynomial	Common [Tropel] Name
1#	1	Piston
2#	$R \cos(\alpha)$	X Tilt
3#	$R \sin(\alpha)$	Y Tilt
4#	$2R^2 - 1$	Power
5*	$R^2 \cos(2\alpha)$	3rd Order Astigmatism
6*	$R^2 \sin(2\alpha)$	3rd Order 45° Astigmatism
7*	$(3R^3 - 2R) \cos(\alpha)$	3rd Order X Coma
8#	$(3R^3 - 2R) \sin(\alpha)$	3rd Order Y Coma
9*	$(6R^4 - 6R^2 + 1$	3rd Order Spherical
10*	$R^3 \cos(3\alpha)$	[3rd Order 3-Point]
11	$R^3 \sin(3\alpha)$	[3rd Order 45° 3-Point]
12*	$(4R^4 - 3R^2) \cos(2\alpha)$	5th Order Astigmatism
13*	$(4R^4 - 3R^2) \sin(2\alpha)$	5th Order 45° Astigmatism
14*	$(10R^5 - 12R^3 + 3R) \cos(\alpha)$	5th Order X Coma
15#	$(10R^5 - 12R^3 + 3R) \sin(\alpha)$	5th Order Y Coma
16*	$20R^6 - 30R^4 + 12R^2 - 1$	5th Order Spherical
17	$R^4 \cos(4\alpha)$	[3rd Order 4-Point]
18	$R^4 \sin(4\alpha)$	[3rd Order 45° 4-Point]
19*	$(5R^5 - 4R^3) \cos(3\alpha)$	[5th Order 3-Point]
20	$(5R^5 - 4R^3) \sin(3\alpha)$	[5th Order 45° 3-Point]
21	$(15R^6 - 20R^4 + 6R^2) \cos(2\alpha)$	7th Order Astigmatism
22	$(15R^6 - 20R^4 + 6R^2) \sin(2\alpha)$	7th Order 45° Astigmatism
23	$(35R^7 - 60R^5 + 30R^3 - 4R) \cos(\alpha)$	7th Order X Coma
24#	$(35R^7 - 60R^5 + 30R^3 - 4R) \sin(\alpha)$	7th Order Y Coma
25	$70R^8 - 140R^6 + 90R^4 - 20R^2 + 1$	7th Order Sphereical
26	$R^5 \cos(5\alpha)$	[3rd Order 5-Point]
27	$R^5 \sin(5\alpha)$	[3rd Order 45° 5-Point]
28	$(6R^6 - 5R^4) \cos(4\alpha)$	[5th Order 4-Point]
29	$(6R^6 - 5R^4) \sin(4\alpha)$	[5th Order 45° 4-Point]
30	$(21R^7 - 30R^5 + 10R^3) \cos(3\alpha)$	[7th Order 3-Point]
31	$(21R^7 - 30R^5 + 10R^3) \sin(3\alpha)$	[7th Order 45° 3-Point]
32	$(56R^8 - 105R^6 + 60R^4 - 10R^2) \cos(2\alpha)$	9th Order Astigmatism
33	$(56R^8 - 105R^6 + 60R^4 - 10R^2) \sin(2\alpha)$	9th Order 45° Astigmatism
34	$(126R^9 - 280R^7 + 210R^5 - 60R^3 + 5R) \cos(\alpha)$	9th Order X Coma
35#	$(126R^9 - 280R^7 + 210R^5 - 60R^3 + 5R) \sin(\alpha)$	9th Order Y Coma
36	$252R^{10} - 630R^8 + 560R^6 - 210R^4 + 30R^2 - 1$	9th Order Spherical
37	$924R^{12} - 2772R^{10} + 3150R^8 - 1680R^6 + 420R^4 - 42R^2 + 1$	11th Order Spherical

Table 1

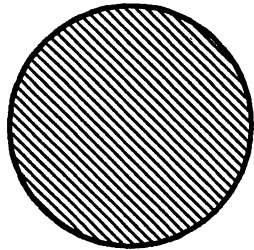## Aerial Image of 0.25 μm Dense Lines
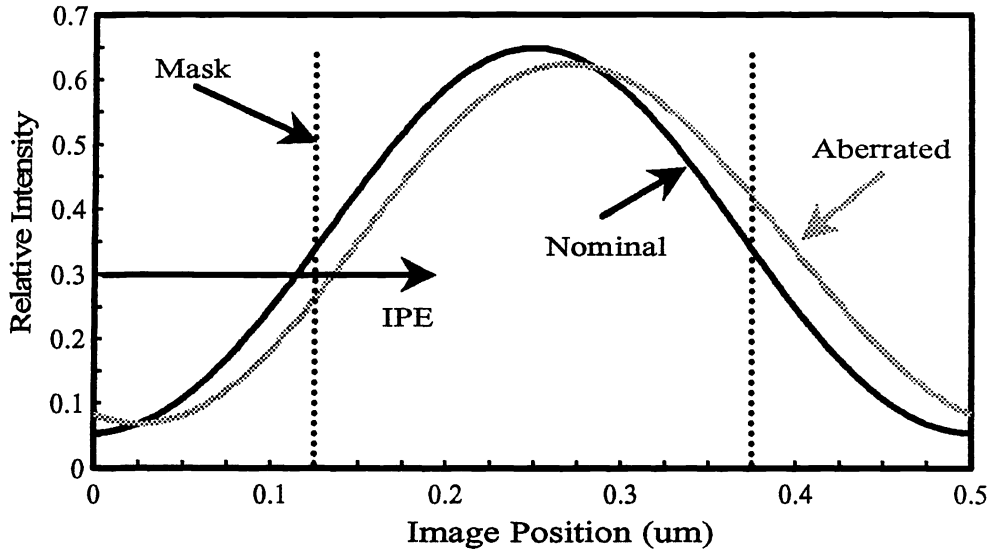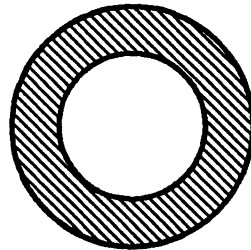

Figure 5

Intensity Distribution in Lens Pupil
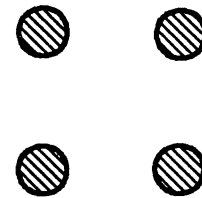
Uniform   Annular   Quadrupole
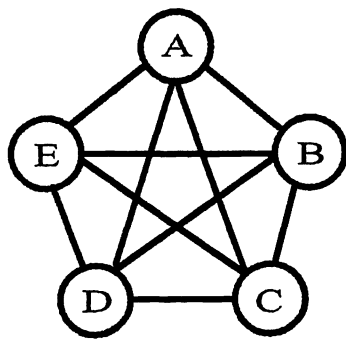

Figure 6

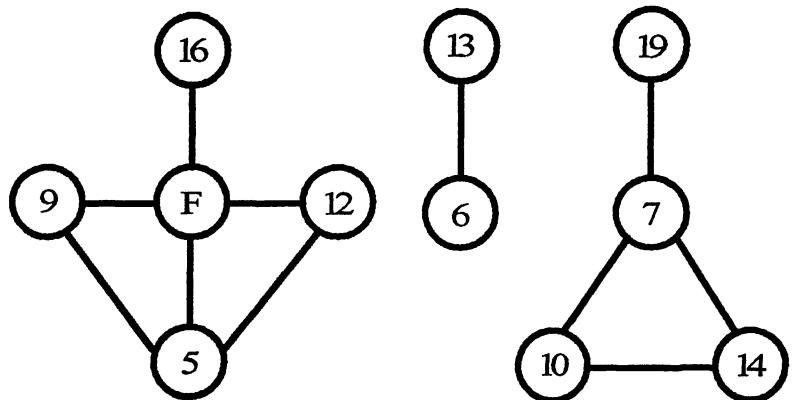## Screening Experiments

Figure 7a

DOE Factors and Interactions

Figure 7b

Relative Influence of DOE Factors

Factor	Total Image Deviation			Symmetry (Right -Left Slope)			Image Placement Error		
	Convent'l	Annular	Quad	Convent'l	Annular	Quad	Convent'l	Annular	Quad
Z5	1.40%	2.08%	0.01%	0.00%	5.19%	3.91%	0.00%	0.00%	0.00%
Z5*Z9	4.33%	0.53%	0.02%	0.01%	2.65%	3.35%	0.01%	0.00%	0.00%
Z5*Z12	1.57%	1.81%	0.01%	0.04%	4.27%	6.56%	0.03%	0.02%	0.00%
Z5*Focus	15.98%	2.35%	0.01%	0.07%	9.32%	9.83%	0.01%	0.01%	0.00%
Z12	0.12%	0.11%	0.00%	0.03%	4.93%	5.19%	0.02%	0.00%	0.00%
Z12*Focus	0.70%	1.60%	0.01%	0.14%	1.10%	3.73%	0.02%	0.00%	0.00%
Z9	6.31%	4.12%	0.00%	0.03%	4.83%	7.35%	0.01%	0.00%	0.00%
Z9*Focus	7.86%	2.14%	0.01%	0.05%	1.81%	7.34%	0.01%	0.00%	0.00%
Z16	1.17%	0.47%	0.04%	0.00%	0.04%	2.68%	0.01%	0.01%	0.00%
Z16*Focus	0.27%	0.15%	0.07%	0.09%	5.61%	1.45%	0.01%	0.01%	0.00%
Focus	2.83%	0.41%	0.00%	0.10%	2.38%	0.37%	0.03%	0.02%	0.00%
Z7	4.04%	1.09%	0.00%	66.62%	4.26%	2.36%	92.61%	77.15%	32.48%
Z7*Z10	0.48%	4.76%	0.08%	0.69%	2.78%	3.89%	0.02%	0.02%	0.00%
Z7*Z14	0.33%	0.32%	0.02%	0.09%	2.84%	3.82%	0.00%	0.01%	0.00%
Z7*Z19	8.54%	3.21%	0.03%	0.14%	2.25%	3.91%	0.00%	0.00%	0.00%
Z10	0.91%	0.73%	0.00%	23.93%	3.61%	0.24%	0.65%	12.88%	15.21%
Z10*Z14	1.02%	1.12%	0.02%	0.04%	3.94%	2.19%	0.01%	0.01%	0.00%
Z14	2.89%	0.69%	0.01%	1.97%	1.25%	0.29%	6.11%	0.05%	8.56%
Z19	1.09%	1.27%	0.00%	5.60%	2.84%	0.92%	0.35%	9.73%	43.75%
Z6	5.78%	10.31%	7.04%	0.00%	3.52%	3.64%	0.01%	0.00%	0.00%
Z13	3.78%	7.03%	13.86%	0.10%	5.67%	2.42%	0.00%	0.00%	0.00%
Z6*Z13	27.33%	52.00%	78.70%	0.07%	0.99%	2.37%	0.01%	0.00%	0.00%
Totals	98.71%	98.30%	99.96%	99.80%	76.08%	77.82%	99.93%	99.95%	100.00%

MIN	0.6267	0.3988	0.0065	-0.3073	-0.0015	-0.0018	-0.0165	-0.0240	-0.0510
MAX	4.5895	4.5986	5.1728	0.2931	0.0015	0.0019	0.0169	0.0246	0.0511

Note: Unshaded areas indicate statistically significant contributions (95% confidence level)
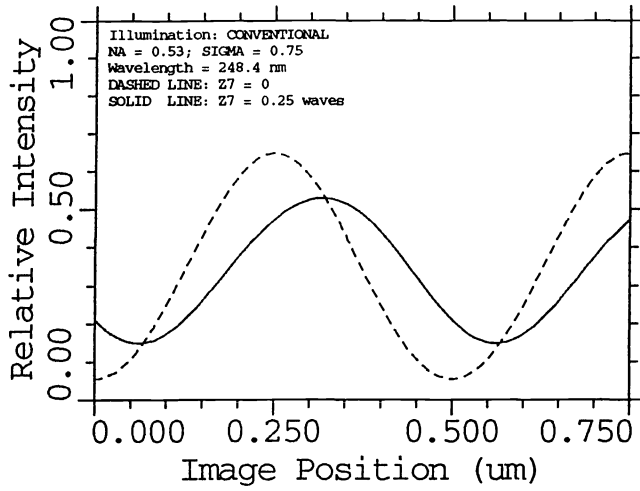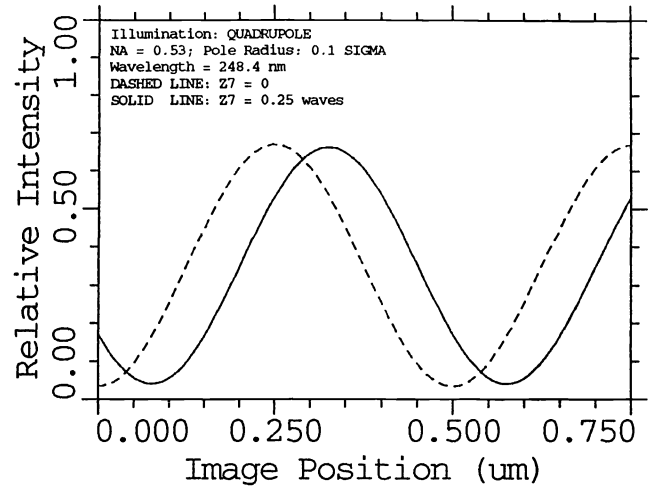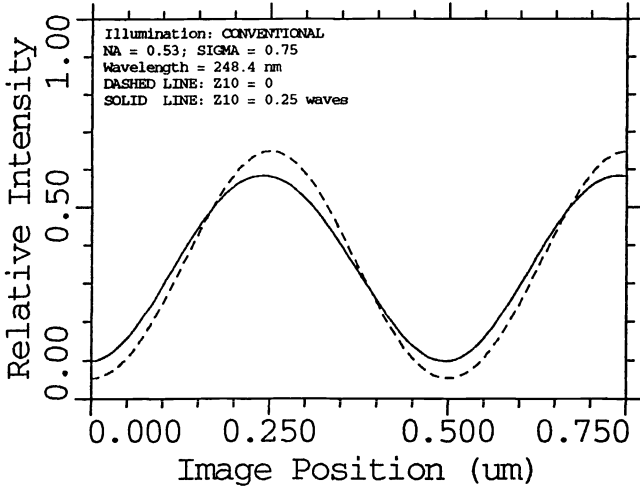
Table 2

Aerial Images of 0.25 um Dense Lines

Illumination: CONVENTIONAL
NA = 0.53; SIGMA = 0.75
Wavelength = 248.4 nm
DASHED LINE: Z7 = 0
SOLID LINE: Z7 = 0.25 waves

Fig 8a.

Illumination: QUADRUPOLE
NA = 0.53; Pole Radius: 0.1 SIGMA
Wavelength = 248.4 nm
DASHED LINE: Z7 = 0
SOLID LINE: Z7 = 0.25 waves

Fig 8b.

Illumination: CONVENTIONAL
NA = 0.53; SIGMA = 0.75
Wavelength = 248.4 nm
DASHED LINE: Z10 = 0
SOLID LINE: Z10 = 0.25 waves

Fig 9a.

Illumination: QUADRUPOLE
NA = 0.53; Pole Radius: 0.1 SIGMA
Wavelength = 248.4 nm
DASHED LINE: Z10 = 0
SOLID LINE: Z10 = 0.25 waves

Fig 9b.

Illumination: CONVENTIONAL
NA = 0.53; SIGMA = 0.75
Wavelength = 248.4 nm
DASHED LINE: Z14 = 0
SOLID LINE: Z14 = 0.25 waves

Fig 10a.

Illumination: QUADRUPOLE
NA = 0.53; Pole Radius: 0.1 SIGMA
Wavelength = 248.4 nm
DASHED LINE: Z14 = 0
SOLID LINE: Z14 = 0.25 waves

Fig 10b.

Aerial Images of 0.25 um Dense Lines

Illumination: CONVENTIONAL
NA = 0.53; SIGMA = 0.75
Wavelength = 248.4 nm
DASHED LINE: Z19 = 0
SOLID LINE: Z19 = 0.25 waves

Fig 11a.

Illumination: QUADRUPOLE
NA = 0.53; Pole Radius: 0.1 SIGMA
Wavelength = 248.4 nm
DASHED LINE: Z19 = 0
SOLID LINE: Z19 = 0.25 waves

Fig 11b.

Illumination: CONVENTIONAL
NA = 0.53; SIGMA = 0.75
Wavelength = 248.4 nm
DASHED LINE: Z5 = 0; Focus = 0
SOLID LINE: Z5 = 0.20 waves; Focus = 0.2 um

Fig 12a.

Illumination: QUADRUPOLE
NA = 0.53; Pole Radius: 0.1 SIGMA
Wavelength = 248.4 nm
DASHED LINE: Z5 = 0; Focus = 0
SOLID LINE: Z5 = 0.20 waves; Focus = 0.2 um

Fig 12b.

Illumination: CONVENTIONAL
NA = 0.53; SIGMA = 0.75
Wavelength = 248.4 nm
DASHED LINE: Z6 = 0; Z13 = 0
SOLID LINE: Z6 = -0.10 waves; Z13 = +0.10 waves

Fig 13a.

Illumination: QUADRUPOLE
NA = 0.53; Pole Radius: 0.1 SIGMA
Wavelength = 248.4 nm
DASHED LINE: Z6 = 0; Z13 = 0
SOLID LINE: Z6 = -0.10 waves; Z13 = +0.10 waves

Fig 13b.

Aerial Images of 0.25 um Dense Lines

Fig 14a.

Illumination: CONVENTIONAL
NA = 0.53; SIGMA = 0.75
Wavelength = 248.4 nm
DASHED LINE: Z9 = 0
SOLID LINE: Z9 = 0.25 waves

Fig 14b.

Illumination: QUADRUPOLE
NA = 0.53; Pole Radius: 0.1 SIGMA
Wavelength = 248.4 nm
DASHED LINE: Z9 = 0
SOLID LINE: Z9 = 0.25 waves
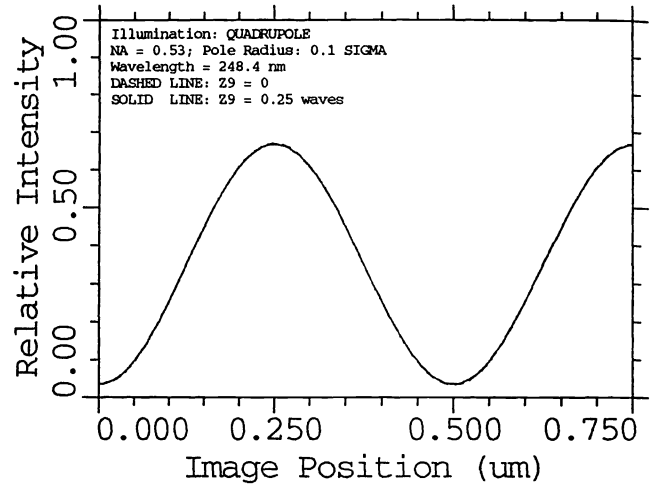
Conventional Illumination
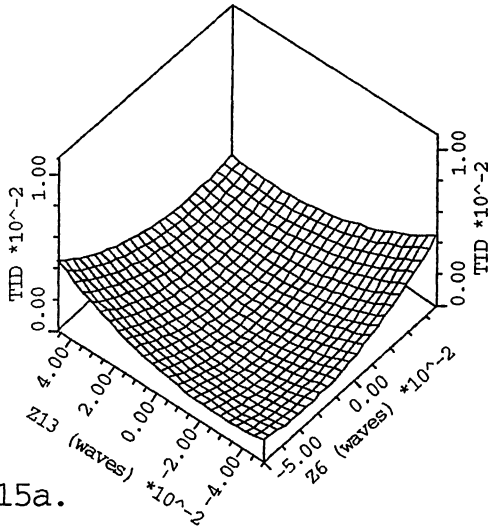
Fig 15a.
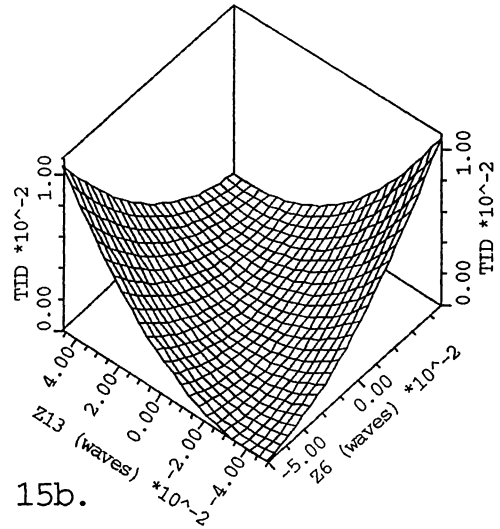
Quad Illumination

Fig 15b.
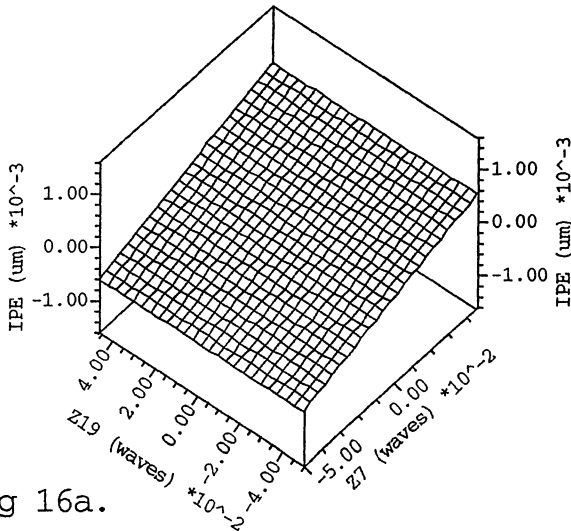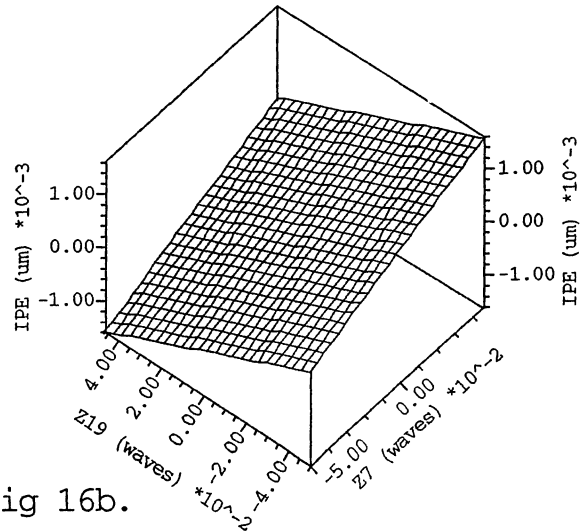
Fig 16a.

Fig 16b.

Conventional Illumination
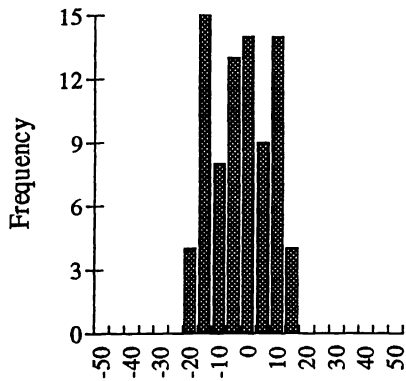
Image Placement Error (nm)

Fig. 17a
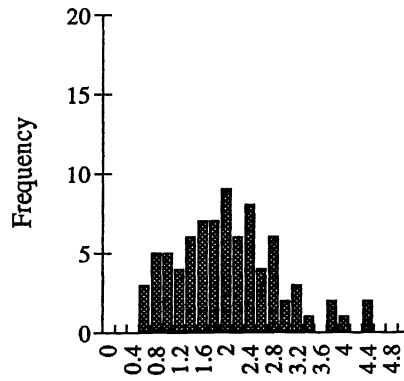
Total Image Deviation

Fig. 18a
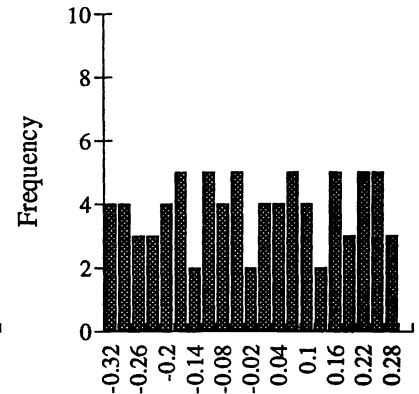
Slope Symmetry

Fig. 19a

Annular Illumination
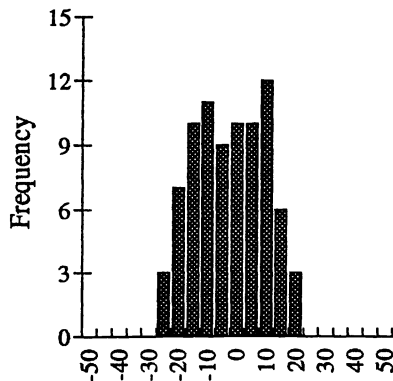
Image Placement Error (nm)

Fig. 17b
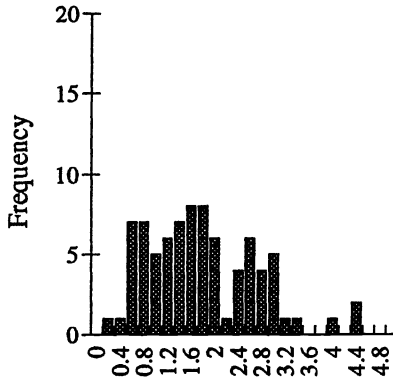
Total Image Deviation

Fig. 18b
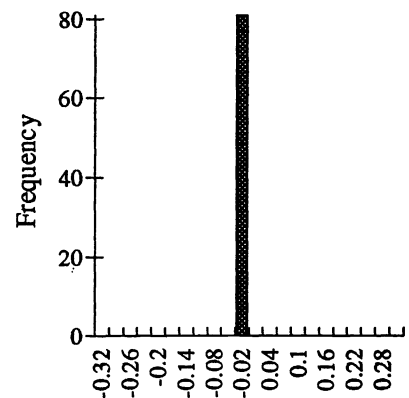
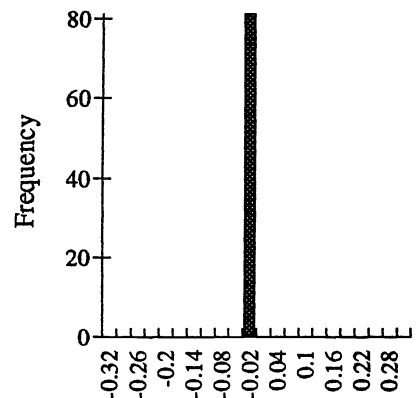Slope Symmetry

Fig. 19b

Quadrupole Illumination
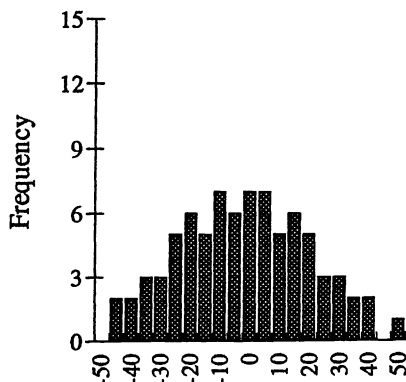
Image Placement Error (nm)

Fig. 17c
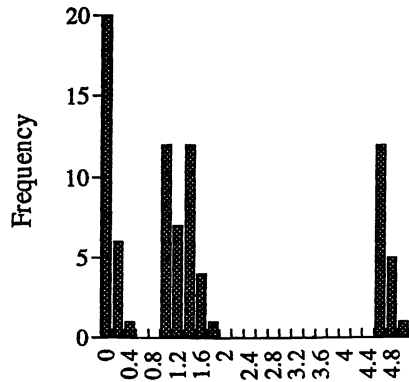
Total Image Deviation

Fig. 18c

Slope Symmetry

Fig. 19c

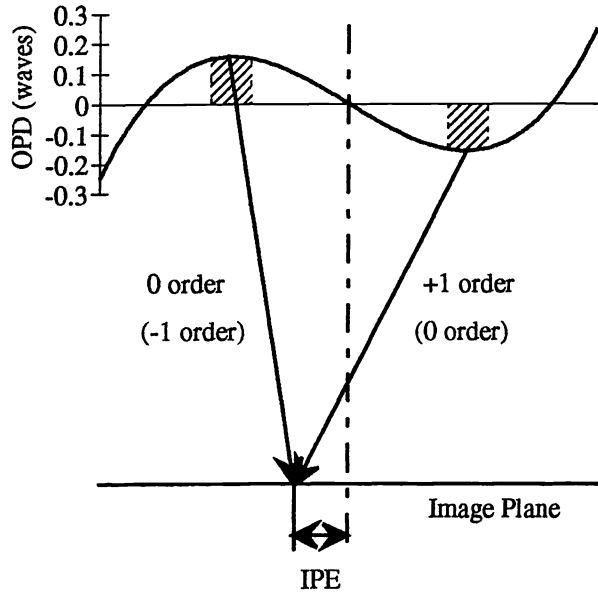## Phase Error Due to 3rd Order Coma (Z7)
(Quadrupole Illumination)

Fig. 20

Radial Image Placement Error
(0.25 um Dense Lines)

Fig. 21

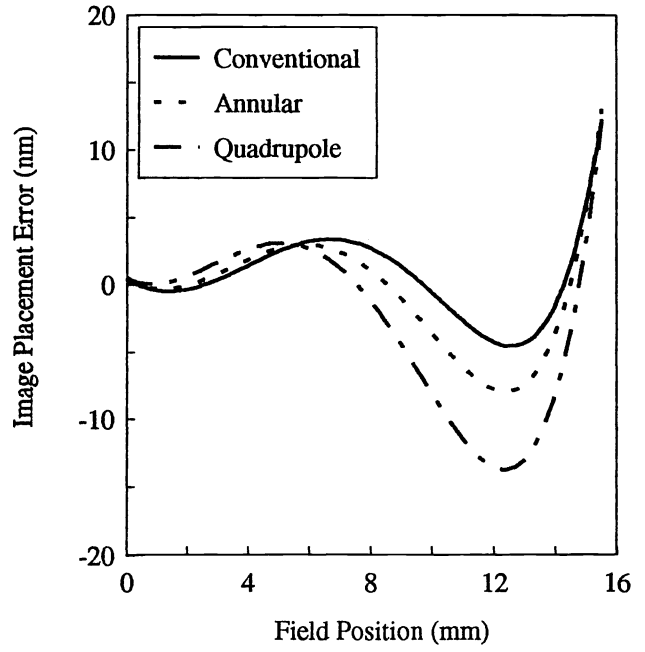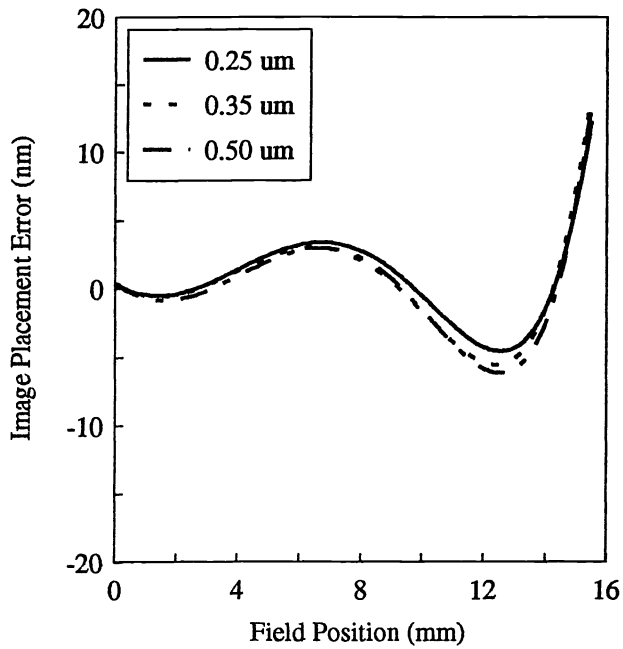## Conventional Illumination

Fig. 22a

Quadrupole Illumination

Fig. 22b